Eur. Phys. J. D **17**, 285–291 (2001)

**THE EUROPEAN PHYSICAL JOURNAL D**

EDP Sciences


# Photoionization cross-sections of the first excited states of sodium and lithium in a magneto-optical trap

V. Wippel[1,a], C. Binder[1], W. Huber[1], L. Windholz[1,b], M. Allegrini[2], F. Fuso[2], and E. Arimondo[2]

[1] Institut für Experimentalphysik, Technische Universität Graz, Petersgasse 16, 8010 Graz, Austria
[2] INFM, Dipartimento di Fisica, Università di Pisa, Via F. Buonarroti 2, 56127 Pisa, Italy

Received 21 March 2001 and Received in final form 3 August 2001

**Abstract.** A two element magneto-optical trap (MOT) for Na and $^7$Li or $^6$Li is used to cool and trap each of them separately. A fraction of the cold atoms is maintained in the first $^2P_{3/2}$ excited state by the cooling laser. These excited state atoms are ionized by laser light in the near-UV region, giving rise to a smaller number of trapped atoms and to different loading parameters. Photoionization cross-sections were derived out of these data. They are in reasonable agreement with data previously obtained using thermal samples and with theoretical predictions.

**PACS.** 32.80.Pj Optical cooling of atoms; trapping – 32.80.Fb Photoionization of atoms and ions

## 1 Introduction

In the last few years magneto-optical traps (MOT) have been used increasingly all over the world as convenient devices for cooling atoms. MOTs are used to provide atoms cooled in and below the mK-range. For instance, spectacular data in MOTs have been obtained for the further cooling towards production of Bose-Einstein condensation [1], for the determination of long range interatomic potentials *via* photoassociation [2–5], and for the formation of long-range molecules [6]. In several MOTs two or more species were simultaneously trapped, either two isotopes of one element [7] or two separate elements [8].

In the present work we report on the operation of a MOT containing sodium or lithium cold atoms. We have used such a MOT as a source of excited atoms for determining the ionization cross-section of the 2 and 3 $^2P_{3/2}$ states of Li or Na, respectively, through photoionization by an additional laser beam. The measurements described here have been carried out with only one element at a time, so that the two species feature of the MOT was not used.

Section 2 describes the different parts of the experimental setup, including the MOT vacuum and optical components. Moreover, the UV lasers required for the photoionization of the two species are specified. Section 3 presents and discusses the main results of our investigation and a comparison with experimental and theoretical cross-section data available in the literature.

[a] e-mail: vw@iep.tu-graz.ac.at
[b] e-mail: l.windholz@iep.tu-graz.ac.at

## 2 Experimental apparatus

### 2.1 MOT

We use a standard MOT working with circular polarized light. The trap consists of a nonmagnetic stainless steel UHV chamber equipped with 10 separate arms allowing for a direct view into the center of the trap where the atom clouds are positioned. The windows are anti-reflection coated. The vacuum chamber is pumped by an ion getter pump, reaching a pressure better than $2 \times 10^{-9}$ mbar. The pressure increases when the dispensers generating the alkali atoms are used, typically $(4-8) \times 10^{-9}$ mbar, depending on the dispenser temperature.

The coils for the magnetic field are located outside the vacuum chamber in a nearly anti-Helmholtz configuration producing a magnetic field gradient of about 2 mT/cm in the center of the trap along the axial direction.

As light sources we use dye ring lasers (Coherent 699-21 and 899-21), pumped by $Ar^+$-ion lasers. The trapping lasers for Na and Li are stabilized by saturation spectroscopy at the cooling laser frequency. The laser light at the cooling frequency for Na (588.995 nm, 100 mW) is spatially filtered by a pinhole before being expanded for the MOT operation. The light at the repumping frequency is produced by an acousto-optic modulator (AOM) running at 1 720 MHz on an auxiliary laser beam. The repumping beam with 15 mW power is expanded and overlapped with the cooling beams in two of the three directions of the laser path.

For lithium-7 (670.776 nm) the repumper is the first order sideband of an EOM driven at 823 MHz with an intensity of approximately 1/3 of the carrier used as the cooling

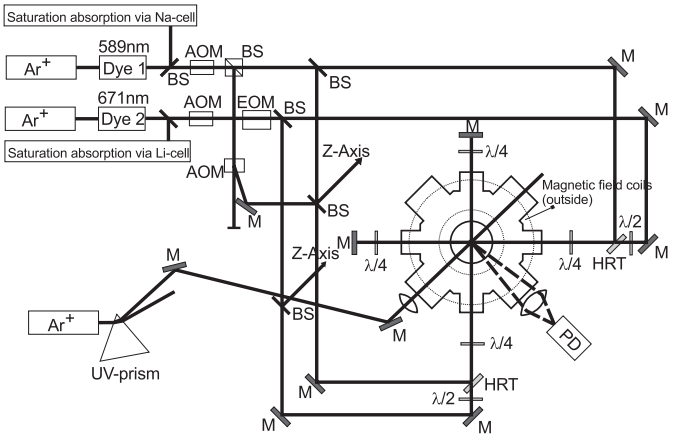


**Fig. 1.** Experimental setup of the Li–Na–MOT. The third $Ar^+$ probe-laser operating in the UV multiline mode is used for the photoionization of the alkali-cloud in the MOT. The UV lines are separated through a prism.

**Table 1.** Center-intensity $I_{0,\max}$ and power of the beam $W_{\max}$ of the UV-laser at its maximum output. $r_e$ is the 1/e-radius of the beam.

| Line [nm] | $I_{0,\max}$ [mW/cm$^2$] | $r_e$ [mm] | $W_{\max}$ [mW] |
|---|---|---|---|
| 334.472$^{(*)}$ ±0.001 | 766 ±15% | 2.0±0.05 | 96 ±5% |
| 335.849$^{(*)}$ | 335 | 2.3 | 56 |
| 351.112$^{(*)}$ | 1 670 | 3.7 | 718 |
| 363.789$^{(*)}$ | 1 820 | 3.0 | 515 |
| 399.5 ±0.1 | 342 ±20% | 1.1±0.05 | 13 ±10% |
| 401.5 | 227 | 1.4 | 14 |
| 402.0 | 670 | 1.0 | 19 |
| 404.0 | 269 | 1.5 | 19 |
| 407.8 | 245 | 1.3 | 13 |

$^{(*)}$ Taken from reference [20] and Laser Innovations/Coherent Laser Systems product specifications.

beam. The second first order sideband is not used, higher order sidebands are not detected. The EOM does not split the produced frequencies spatially, so no further steps to overlap the beams are required. The laser power including all EOM-bands for all three directions is typically 80 mW. The laser for $^6$Li cooling works at 670.791 nm, the repumping frequency is produced by double-passing an AOM at 109 MHz. The repumper power is 10 mW, the cooling power is 40 mW.

The optical arrangement can be seen in Figure 1. The AOMs and EOM are used to obtain sidebands, for frequency stabilization and for chopping. Each beam is expanded to 25 mm diameter and split spatially into three beams of approximately equal intensity by appropriate beam-splitters (BS). Each lithium laser-beam passes a $\lambda/2$-plate to rotate the polarization by $\pi/2$, because we use one quarter wave plate for both wavelengths, showing different phase shifts for 589 nm and 671 nm. The red and the yellow light beams are combined by three dichroic mirrors (HRT), then each of the three combined laser beams gets through a $\lambda/4$-plate, passes the trap, one more $\lambda/4$-plate and gets retro-reflected by a mirror (M). The outgoing beams can easily be overlapped by the incoming beams at the entrance aperture. The back-reflected beams are generally intentionally misaligned by a few mrad to avoid interferences. This decreases the fluorescence of the cloud, but also considerably diminishes the fluctuations of its fluorescence and position. The angle alignment of the $\lambda/4$-plates is not sensitive, the Na MOT worked even with two of the three entrance $\lambda/4$-plates removed.

The fluorescence intensity of the clouds of trapped atoms is measured by a photodiode (PD).

The dispensers producing the sodium and lithium atoms are from SAES Getters, Italy. They are in the size of matches, one containing Na, the other Li. No information about purity, isotope distribution and additional substances is available to us. Two sets are mounted inside the vacuum chamber: the first one 5 cm from the center of the trap, the other one 20 cm above the cloud, with no direct view onto it. That second dispenser is used to avoid an influence on the cold atoms by the emitted hot atoms. After initial outgassing, heating, and use at currents higher than the normal ones for several minutes, the dispensers can be used in UHV. The current can be varied to obtain more or less Na or Li in the vapor, leading to clouds with different numbers of atoms. The dispensers above the cloud operate at higher currents in order to create the required background alkali pressure in the trapping region. Because both dispensers are heated strongly, glowing faintly red, the temperature of the emitted atoms is high, and only a few atoms are in the slow motion range of the Maxwellian distribution so to be captured by the MOT.

The experimental arrangement is designed to trap Na and Li simultaneously. This feature is not used in the present work.

## 2.2 Photoionization

For the photoionization experiments an $Ar^+$-ion laser is used in UV-multiline mode. Using a quartz prism, the different lines are separated. Some UV-wavelengths for ionizing sodium are produced by a dye ring laser working with Exalite 402 around 400 nm. As this laser has a smaller intensity than the $Ar^+$-ion laser, the beam is compressed using two lenses.

The Gaussian profile of the laser beams was recorded to calculate the peak intensity $I_0$. For some measurements a UV-photodiode with a very small aperture was scanned through the UV-beam. The beams proved to be Gaussian with a beam radius $r_e$ above 1 mm (Tab. 1). So for our atom clouds with a diameter below 0.3 mm the intensity is supposed to be uniform with the value of $I_0$ within a few %. Apertures could not be used to delimit the beam diameter in order to control the interactions between the photoionization laser and the background vapor, interactions discussed in references [9,10]. In effect those apertures produced distinct diffraction fringes even at apertures larger than 5 mm. Using both a laser power-meter

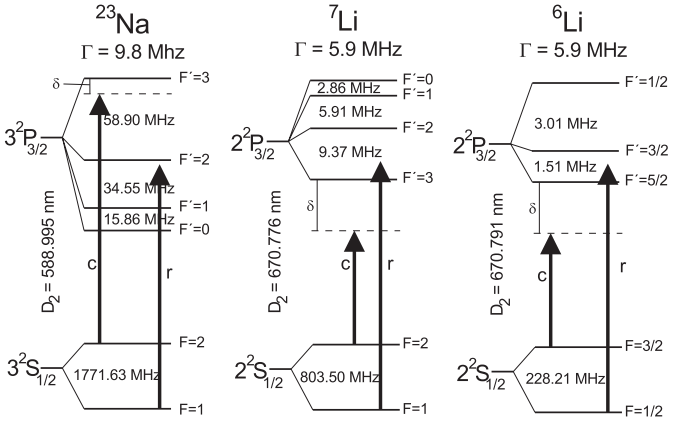


**Fig. 2.** Energy levels for $^{23}$Na, $^{7}$Li, and $^{6}$Li, and cooling (c) and repumping (r) laser frequencies used in the double MOT. Wavelengths (for air) and frequencies calculated from data out of reference [12].

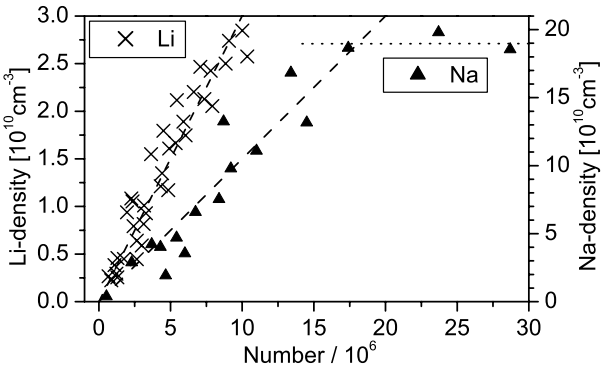


**Fig. 3.** Number $N$ of atoms and $n_0$, density in the center, of cold Na- and $^{7}$Li-clouds measured separately. The dashed lines represent the expected $n(N)$ dependence for the case of the temperature-limited regime with a constant volume. At high $N$, the Na data reach the density limited region with a constant density, denoted by a horizontal dotted line.

and a thermopile, the photoionization intensity was measured. This leads to similar results within a few %. This is also valid when using the UV-photodiode as an additional way of measuring the UV-intensity through calibration of the diode.

## 3 Results and discussion

For $^{7}$Li and $^{23}$Na ($n = 2, 3$ respectively) the cooling transition is $n^2\mathrm{S}_{1/2}(F = 2) \rightarrow n^2\mathrm{P}_{3/2}(F' = 3)$, the repumping transition is $n^2\mathrm{S}_{1/2}(F = 1) \rightarrow n^2\mathrm{P}_{3/2}(F' = 2)$. For $^{6}$Li we use $2^2\mathrm{S}_{1/2}(F = 3/2) \rightarrow 2^2\mathrm{P}_{3/2}(F' = 5/2)$ and $2^2\mathrm{S}_{1/2}(F = 1/2) \rightarrow 2^2\mathrm{P}_{3/2}(F' = 3/2)$, respectively. For lithium it should be taken into account that the hyperfine splitting is smaller than the natural linewidth, as can be seen in the level diagrams of Figure 2. We chose the laser frequencies corresponding to a detuning of the cooling beams of (10 and 25) MHz to the red, and for the repumpers (3 and 15) MHz for Na and $^{7}$Li, respectively.

The cloud was observed by using a CCD camera. Fitting a Gaussian profile to the cross-section of the picture of the cloud allowed us to derive $r_{x,e}$, the 1/e-radius of the cloud. In our case this is a radial direction, so the value for the axial direction is $r_e = r_{x,e}/\sqrt{2}$. This value is connected with $r_\mathrm{T}$ used in reference [14] by $r_\mathrm{T} = r_e/\sqrt{2} = r_{x,e}/2$.

The fluorescence intensity $I$ emitted by the cold atoms was measured by a calibrated photodiode. The number of cold atoms $N_0$ in the cloud was determined by the following relation:

$$N_0 = I/(h\nu\, \Gamma\eta\Pi^{(e)}). \qquad (1)$$

Here $h\nu$ is the energy of a laser photon, $\Gamma$ the linewidth of the transition, $\eta$ a geometry factor of the imaging system and $\Pi^{(e)}$ the fraction of excited atoms at the given laser intensity and detuning. We calculated the fraction of excited atoms $\Pi^{(e)}$ by using the models reported in references [13,14]. The formulas of [13,14] have been modified according to the angular momenta of the level scheme mentioned above, and using of the appropriate detuning and intensities of the trapping lasers.

Assuming the cloud of the MOT being elliptically symmetric with a Gaussian profile, the local density $n_0$ in the center can be calculated.

An estimation of the temperature $T$ for the cold atoms was obtained with the release-capture method, *i.e.* by fitting the fraction $f_\mathrm{r}$ of atoms remaining in the trap, dependent on the shut off time $\Delta t$ of the cooling lasers, through the following formula [13]:

$$f_\mathrm{r} = \mathrm{erf}\left(\frac{v_\mathrm{c}}{v_\mathrm{th}}\right) - \frac{2}{\sqrt{\pi}}\left(\frac{v_\mathrm{c}}{v_\mathrm{th}}\right)\exp\left(-\left(\frac{v_\mathrm{c}}{v_\mathrm{th}}\right)^2\right). \qquad (2)$$

This relation describes the expansion of a Maxwellian distributed cloud neglecting its extension and the influence of gravity. $v_\mathrm{th}$ is the mean thermal velocity and $v_\mathrm{c} = R_\mathrm{c}/\Delta t$ the velocity necessary for an atom to cross the laser beam with the radius $R_\mathrm{c}$ in the time interval $\Delta t$ [13]. erf () is the Gaussian error function. For $^{7}$Li as well as for Na we measured a temperature of (200−300) $\mu$K. The value has to be considered as a lower limit, because we were not able to switch off the magnetic field fast enough. So, especially for Li, magnetic forces may slow down the escape of atoms out of the trap.

### 3.1 MOT without UV

The number of atoms and the density of the Na and Li clouds depends on the cooling-laser intensity and detuning and on the dispenser current. Varying these parameters, we were able to explore the dependence of atomic density on the number of cold atoms in the trap, as shown in Figure 3. We trapped only some thousands of $^{6}$Li atoms due to their small occurrence in natural Li. So $^{6}$Li is not shown in Figure 3.

The influence of the dispenser current on the number of atoms, as well as the partial pressure and the temperature of the alkaline vapor emitted was not examined quantitatively.

The experimental results of Figure 3 indicate that for a large range of operating conditions the clouds of each element were in the temperature-limited regime where the cloud volume is constant and the density linear with the number of atoms. In the region above $1.5 \times 10^7$ Na atoms the density curve bends into a constant-density regime. The fits of a Gaussian distribution to the spatial distributions of the atoms lead for the Na-cloud to an 1/e-radius in the radial direction of typically 0.15 mm and for the Li-cloud to 0.4 mm. The Na-cloud is definitely smaller with a higher density, indicating its lower temperature compared to Li. In the temperature-limited regime the radius $r_i$ along each axis ($i = x, y, z$) is given by the equipartition theorem [14]

$$\frac{1}{2}\kappa_i r_{T,i}^2 = \frac{1}{2}k_{\mathrm{B}}T \tag{3}$$

with $\kappa_i$ the spring constant along that axis, and the relation $\kappa_z = 2\kappa_x = 2\kappa_y$ between the different axes in a quadrupole magnetic trap. If we apply the empirical relation $\kappa_z = \kappa_0 \times (\Gamma/\delta) \times (b/b_0)$ of reference [14] with $b$ the magnetic field gradient and $b_0$ a constant taken as 0.1 mT/cm, we are able to give an estimation for $\kappa_0$ in Na and Li. Taking 250 $\mu$K as lower temperature limit, for Na $\kappa_0$ calculates to $\kappa_0 \geq 3 \times 10^{-20}$ N/m, for Li $\kappa_0 \geq 2 \times 10^{-20}$ N/m. These values have to be taken as a first hint because of the systematic errors mentioned above. They are comparable to those derived for rubidium and cesium in [14].

The loading time is (3–6) s for 90% fluorescence for both elements. The decay lifetime could not be measured because the dispensers could not be switched off fast enough.

### 3.2 Photoionization

Irradiation of the excited fraction of a cold atomic sample (Na: $3\,\mathrm{P}_{3/2}$, Li: $2\,\mathrm{P}_{3/2}$) by laser photons with an energy above the ionization threshold leads to observable effects in the MOT loading process. This can be used to derive the relevant ionization cross-sections. Without a photoionization beam for a MOT operating in the density-limited regime, *i.e.* with a constant density $n$ of trapped atoms, the loading curve is described by an exponential growth. That growth is determined by the balance between the loading rate and a loss rate $\gamma$. $\gamma$ accounts for collisions with background gas particles with a rate $\gamma_{\mathrm{B}}$, and with collisions with atoms in the MOT with a rate $\beta n$

$$\gamma = \gamma_{\mathrm{B}} + \beta n. \tag{4}$$

In these conditions the steady state number of trapped atoms $N_0$ is given by

$$N_0 = \frac{L_0}{\gamma}, \tag{5}$$

$L_0$ being the actual loading rate of the trap.

Following the treatment presented, for instance, in references [9,10], photoionization opens a new trap loss channel with a rate $\gamma_{\mathrm{P}}$. For a single photon process neglecting saturation effects $\gamma_{\mathrm{P}}$ is given by

$$\gamma_{\mathrm{P}} = \Pi^{(e)}\frac{\sigma_{\mathrm{P}} I_{\mathrm{P}}}{h\nu_{\mathrm{P}}}, \tag{6}$$

where $\sigma_{\mathrm{P}}$ is the cross-section, $I_{\mathrm{P}}$ the photoionization laser intensity, and $h\nu_{\mathrm{P}}$ the photon energy. The $\gamma_{\mathrm{P}}$ rate adds up to the loss rate $\gamma$ leading to the total loss rate

$$\gamma_{\mathrm{t}} = \gamma + \gamma_{\mathrm{P}}. \tag{7}$$

Moreover, photoionization of excited alkali atoms in the background is expected to modify the loading dynamics. As a consequence, in the presence of a photoionization beam the loading rate becomes $L_{\mathrm{P}} = L_0 \exp(-\gamma_{\mathrm{P}}\tau_{\mathrm{C}})$, $\tau_{\mathrm{C}}$ being related to the characteristic time for an atom to be captured in the MOT [9,10]. The steady state value for the number of atoms $N_{\mathrm{P}}$ in the presence of photoionization can then be written as

$$N_{\mathrm{P}} = N_0 \frac{\mathrm{e}^{-\gamma_{\mathrm{P}}\tau_{\mathrm{C}}}}{1 + \gamma_{\mathrm{P}}/\gamma}\,. \tag{8}$$

Thus, the number $N(t)$ of atoms in a density-limited MOT at the time $t$ is given by

$$N(t) = N_{\mathrm{P}}(1 - \mathrm{e}^{-\gamma_{\mathrm{t}}t}). \tag{9}$$

For a MOT operating in the temperature-limited regime, *i.e.* with a constant volume $V$, as in some of the measurements presented here, the relevance of two-body collisions between trapped atoms leads to a nonexponential loading behavior [15]. Here equation (7) is valid with $\gamma = \gamma_{\mathrm{B}} + \beta$, and $\gamma_{\mathrm{P}}$ from equation (6). The time dependent number of trapped atoms is

$$N(t) = L_{\mathrm{P}}\frac{2(1 - \mathrm{e}^{-\gamma_{\mathrm{e}}t})}{\gamma_{\mathrm{e}} + \gamma_{\mathrm{t}} + (\gamma_{\mathrm{e}} - \gamma_{\mathrm{t}})\mathrm{e}^{-\gamma_{\mathrm{e}}t}} \tag{10}$$

where

$$\gamma_{\mathrm{e}} = \sqrt{\gamma_{\mathrm{t}}^2 + 4\beta L_{\mathrm{P}}/V}\,, \quad V = r_x r_y r_z \pi^{3/2}. \tag{11}$$

However, this nonexponential character of equation (10) cannot be seen when fitting the loading curves with this function. Both fits, the density- and temperature-limited, seem to approximate the loading curve quite well within the noise. So for further evaluations we used the exponential function (Eq. (9)) due to simplicity.

Information on both the time evolution and the steady state number of trapped atoms can be readily acquired by monitoring the fluorescence emission from the MOT during a loading cycle. One loading curve with and without the photoionization trap loss is shown in Figure 4, referring to the Na MOT irradiated with $\lambda_{\mathrm{P}} = 364$ nm at $I_{\mathrm{P}} = 490$ mW/cm$^2$; modifications produced in the time behavior and in the steady state value can easily be seen. Fitting those curves with equation (9) for measurements carried out with the MOT operating in the

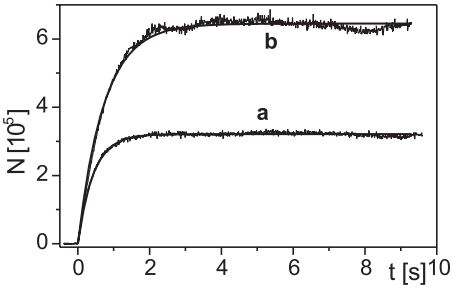


**Fig. 4.** Loading curve of Na in a MOT with (**a**, lower curve) and without (**b**, upper curve) a photoionization beam at $\lambda_P = 364$ nm, $I_P = 490$ mW/cm$^2$. Best fits according to equation (9) are superimposed to experimental data.

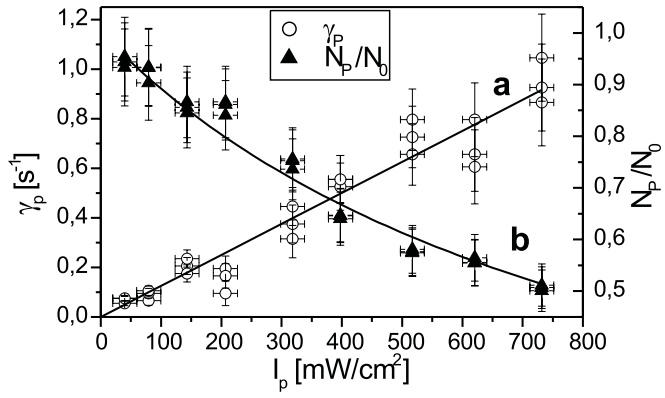


**Fig. 5.** Loss rate $\gamma_P$ and ratio $N_P/N_0$ as a function of the photoionization UV-laser intensity $I_P$. $N_0$ and $N_P$ are the steady state numbers of atoms without any UV-light and with UV-light at $I_P$, respectively. The continuous lines represent best fits according to the equations discussed in the text. Data refer to photoionization with $\lambda_P = 334$ nm, $\sigma = 2.2$ Mbarn, $\tau_C = 86$ ms. Results for three different sets of measurements are superimposed.

density- and temperature-limited regimes, allowed us to derive the steady state number of atoms and the $\gamma$ and $\gamma_P$ rates. We measured $\gamma$ values between 0.5 s$^{-1}$ and 1.4 s$^{-1}$, depending on the dispenser current. Analysis of the initial slope of the loading curves enabled the derivation of the loading rate $L_P = dN/dt$ ($t \approx 0$).

The dependence of $\gamma_P$ and $N_P/N_0$ on the photoionization laser intensity $I_P$ for the case of the Na MOT are shown in Figures 5a and 5b, respectively. The reported error bars for $\gamma_P$ are derived according to the best fit procedure, whereas those for $N_P/N_0$ reflect essentially the fluctuations in the steady state number of atoms during the MOT operation. Results for three different sets of measurements, all under the same conditions, one directly after the other, are shown in order to have an idea of the repeatability of the results. Equation (6) enabled us to directly evaluate the absolute photoionization cross-section $\sigma_P$ from $\gamma_P$ data of Figure 5a.

Equation (8) can also be used to derive the cross-section from the $N_P/N_0$ data of Figure 5b. In this equation $\tau_C$ is a fitting parameter, too. Being strongly correlated with $\sigma_P$ and not sensitive to changes, it proves to be a bad variable to fit. So a large range of values seem to produce a reasonable fit to the data. Therefore, the $\sigma_P$-values presented in the following were only derived fitting $\gamma_P$ with equation (6). We derived values for $\tau_C$ using equation (8) and fixing $\sigma_P$ in that equation to the value obtained from the $\gamma_P$-fit based on equation (6). However, in this case too the $\tau_C$-values do not seem to be significant.

**Table 2.** Photoionization cross-sections $\sigma_P$ of the first excited states of Na and Li for applied UV-radiation of wavelength $\lambda$. $\sigma$ is the average value of 8–10 measurements, reported with a square in Figure 6.

| $\lambda$ [nm] | Atom | $\sigma_P$ [Mbarn] |
|---|---|---|
| 334.472 | Na | $3.1 \pm 0.6$ |
| 335.849 | Na | $2.8 \pm 0.6$ |
| 351.112 | Na | $1.2 \pm 0.2$ |
| 363.789 | Na | $3.7 \pm 0.7$ |
| 399.5 | Na | $8.4 \pm 1.3$ |
| 401.5 | Na | $7.1 \pm 1.1$ |
| 404.0 | Na | $9.1 \pm 1.4$ |
| 407.8 | Na | $6.9 \pm 1.0$ |
| 334.472 | $^7$Li | $16.2 \pm 2.5$ |
| 335.849 | $^7$Li | $18.3 \pm 2.8$ |
| 334.472 | $^6$Li | $15 \pm 15$ |
| 335.849 | $^6$Li | $6(-5, +20)$ |

As shown in Figure 5, a fairly good agreement between experimental data and best fit lines is obtained. In particular, the behavior of $\gamma_P$ as a function of $I_P$ is well described by a linear slope for all measurements presented here. In references [10,11] it was shown that deviations from the linear dependence of $\gamma_P$ *versus* $I_P$ could reveal the occurrence of processes involving recombination and charge diffusion during photoionization of Cs and Rb MOTs. These processes are essentially related to the formation of a relatively cold and dense plasma, in conditions which appear to be not achieved in the present experiment with Na and Li atoms. Na photoionization was also accomplished by using laser wavelengths close to the threshold (Tab. 1), leading to the production of relatively cold electrons (electron excess energy below 100 meV), comparable to those achieved in the Cs experiment of reference [10]. In our case, the limited intensity available for the ionization process resulted in a negligible contribution of the recombination process.

For sodium several laser wavelengths were available for photoionization, leading to the cross-section values reported in Table 2. As shown in Figure 6 these values are in reasonable agreement with the theoretical predictions of [16]. Furthermore, that reference also reported experimental results for an investigation with a synchrotron radiation source, in quite good agreement with the theoretical predictions. The data shown as squares in Figure 6 belong to a series of measurements where the UV-power was measured by using a powermeter; for the data shown as crosses a UV-photodiode was used for the measurement.

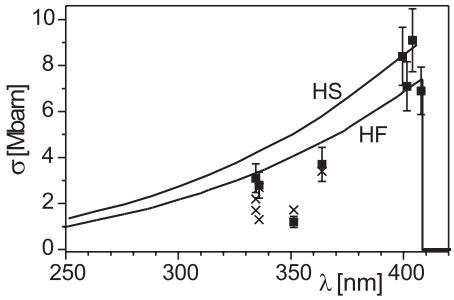


**Fig. 6.** Cross-sections $\sigma_P$ with respect to the ionizing wavelength $\lambda_P$ for Na $3\,P_{3/2}$. The squares are obtained as average over several values, the crosses are measurements with a different method to determine the UV-intensity. The solid lines represent results of the theoretical calculation of reference [16] HF by Hartree-Fock and HS by Hartree-Slater. The experimental data of [16] lie within these lines in the range 300–400 nm.

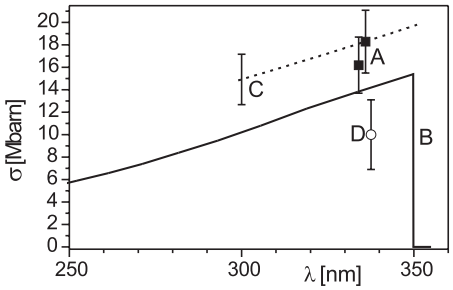


**Fig. 7.** Cross-sections $\sigma_P$ with respect to the ionizing wavelength $\lambda_P$ for $^7$Li $2\,P_{3/2}$. Our data (A) are the black squares, the solid line (B) represents results of the theoretical calculation of reference [17]. The dashed line (C) represents the experimental results of reference [18] with an indicative error bar, while the hollow dot (D) represents the measurement of reference [19].

For the 334 nm and 336 nm wavelengths some measurements based on the UV-photodiode, crosses in Figure 6, produced cross-section values much lower than all the others at the same wavelength. We suppose that the difference is related to an error in the UV-photodiode calibration. For the cross-section at $\lambda_P = 351$ nm we measured a value lower than the predicted one, with both power measurement systems, based on the power-meter and on the UV-photodiode. A careful check of the experimental parameters could not explain why that value was so low in all our measurements. Unfortunately, no additional wavelength close to 351 nm was available to test the presence of a resonance (molecular resonance?) in the photoionization spectrum.

Since the location of the cloud of cold atoms is slightly influenced by unbalances in the intensities of the cooling/repumping laser beams, our trapped atoms may feel magnetic fields up to 0.1 mT (estimated from a shift of 0.5 mm from the trap center and a field gradient of 2 mT/cm). The shift also causes a different orientation of the atoms, while the ionizing laser beam was always linear polarized in the same direction. Such an effect should not influence the measured value of $\gamma_P$.

Error bars of our cross-section measurements are relatively large (typically larger than $\pm 15\%$), for instance larger than those reported in the cesium investigation [9]. The size of the error arises essentially from MOT instabilities, larger in the sodium of the present work than in the previous cesium study. Furthermore, it is caused by the use of UV lines for the sodium photoionization, whose intensities could not be measured precisely enough. Finally, it must be noted that the "hot" sodium experimental data we are comparing to are more accurate than those previously available for "hot" cesium.

Cross-section data for $^7$Li are shown in Figure 7 corresponding to the photoionization laser wavelengths available in this case. Both lithium isotopes have the same cross-section within the error bars, about 17 Mbarn for $\lambda_P = 335$ nm. Our measured values are not too far from the theoretical predictions derived in [17]. The dashed line in Figure 7 represents the experimental results of [18], with a representative error bar, while the hollow dot represents the experimental result of [19]. The error bars of our investigation are comparable to those realized in these previous experimental investigations on thermal samples too.

The absolute values of the photoionization cross-sections depend on the size of the fraction of excited states, $\Pi^{(e)}$. Within the assumed models of [13,14] the error of $\Pi^{(e)}$ is mainly due to uncertainties of the intensity in the cooling laser profile. For the evaluation of the ionization cross-section it is negligible compared to other contributions. However the use of different models describing the interactions of cold atoms with the pumping laser could lead to different values of $\Pi^{(e)}$, hence different values of the photoionization cross-sections [21].

## 4 Conclusions and outlook

Na and $^7$Li or $^6$Li were trapped and cooled in a MOT independently. The trapped atoms in the first excited state were ionized using UV-laser radiation. Measurements of the loading curves allowed us to evaluate the cross-section of the photoionization process. Both Na and Li cross-sections are in agreement with the theoretical predictions, confirming like the previous rubidium and cesium investigations that cold atom photoionization is a flexible technique. While an improvement in the accuracy of the photoionization data can be realized using intense UV radiation sources as in reference [16], the present investigation reaffirms the flexibility offered by the cold atom samples as targets for atomic physics experiments.

The Austrian part of this work is funded by the Austrian Science Foundation (FWF), project numbers P11877, P14645, while the Italian one is funded by the INFM through PRA and PAIS initiatives. E.A. wishes to thank S.T. Manson for useful discussions on the cross-sections data.

## References


1. M. Anderson, J. Ensher, M. Matthews, C. Wieman, E. Cornell, Science **269**, 198 (1995); K. Davis, M. Mewes, M. Andrew, N. Vandruten, D. Durfee, D. Kurn, W. Ketterle, Phys. Rev. Lett. **75**, 3969 (1995); C. Bradley, C. Sackett, R. Hulet, Phys. Rev. Lett. **78**, 985 (1997).
2. For Li see E. Abraham, N. Ritchie, W. McAlexander, R. Hulet, J. Chem. Phys. **103**, 7773 (1995); E. Abraham, W. McAlexander, H. Stoof, R. Hulet, Phys. Rev. A **53**, 3092 (1996).
3. For Na see V. Bagnato, L. Marcassa, C. Tsao, Y. Wang, J. Weiner, Phys. Rev. Lett. **70**, 3225 (1993); L. Ratliff, M. Wagshul, P. Lett, S. Rolston, W. Phillips, J. Chem. Phys. **101**, 2638 (1994); P. Molenaar, P. van der Straten, H. Heideman, Phys. Rev. Lett. **77**, 1460 (1996); J. Blange, J. Zijlstra, A. Amelin, X. Urbain, H. Rudolph, P. van der Straten, H. Beijerinck, H. Heideman, Phys. Rev. Lett. **78**, 3089 (1997).
4. For K see H. Wang, P. Gould, W. Stwalley, Phys. Rev. A **53**, R1216 (1996); H. Wang, P. Gould, W. Stwalley, J. Chem. Phys. **106**, 7899 (1997).
5. For Rb see J. Miller, R. Cline, D. Heinzen, Phys. Rev. Lett. **71**, 2204 (1993); R. Cline, J. Miller, D. Heinzen, Phys. Rev. Lett. **73**, 632 (1994).
6. A. Fioretti, D. Comparat, A. Crubellier, O. Dulieu, F. Masnou-Seeuws, P. Pillet, Phys. Rev. Lett. **80**, 4402 (1998).
7. W. Süptitz, G. Wokurka, F. Strauch, P. Kohns, W. Ertmer, Opt. Lett. **19**, 1571 (1994); M.O. Mewes, G. Ferrari, F. Schreck, A. Sinatra, C. Salomon, Phys. Rev. A **61**, 011403 (2000).
8. M.S. Santos, P. Nussenzveig, L.G. Marcassa, K. Helmerson, J. Flemming, S.C. Zílio, V.S. Bagnato, Phys. Rev. A **52**, R4340 (1995); W. Scherf, V. Wippel, T. Fritz, D. Gruber, L. Windholz, Europhys. Conf. Abstr. D **22**, 6 (1998); G.D. Telles, L.G. Marcassa, S.R. Muniz, S.G. Miranda, A. Antunes, C. Westbrook, V.S. Bagnato, Phys. Rev. A **59**, R23 (1999); J.P. Shaffer, W. Chapulpczak, N.P. Bigelow, Phys. Rev. Lett. **82**, 1124 (1999); Phys. Rev. A **60** R3365 (1999); U. Schlöder, H. Engler, U. Schünemann, R. Grimm, M. Weidemüller, Eur. Phys. J. D **7**, 331 (1999); G.D. Telles, W. Garcia, L.G. Marcassa, V.S. Bagnato, D. Ciampini, M. Fazzi, J.H. Müller, D. Wilkowski, E. Arimondo, Phys. Rev. A **63**, 033406 (2001).
9. O. Maragò, D. Ciampini, F. Fuso, E. Arimondo, C. Gabbanini, S.T. Manson, Phys. Rev. A **57**, R4110 (1998), and references therein.
10. F. Fuso, D. Ciampini, E. Arimondo, C. Gabbanini, Opt. Commun. **173**, 223 (2000).
11. S. Kulin, T.C. Kilian, S.D. Bergeson, S.L. Rolston, Phys. Rev. Lett. **85**, 318 (2000).
12. W. Scherf, O. Khait, H. Jäger, L. Windholz, Z. Phys. D **36**, 31 (1996).
13. P. Molenaar, Ph.D. thesis, Universiteit Utrecht, 1996.
14. C.G. Townsend, N.H. Edwards, C.J. Cooper, K.P. Zetie, C.J. Foot, A.M. Steane, P. Szriftgiser, H. Perrin, J. Dalibard, Phys. Rev. A **52**, 1423 (1995).
15. A. Browaeys, J. Poupard, A. Robert, S. Nowak, W. Rooijakkers, E. Arimondo, L. Marcassa, D. Boiron, C.I. Westbrook, A. Aspect, Eur. Phys. D **8**, 199 (2000).
16. J.M. Preses, C.E. Burkhardt, R.L. Corey, D.L. Earsom, T.L. Daulton, W.P. Garver, J.J. Leventhal, A.Z. Msezane, S.T. Manson, Phys. Rev. A **32**, 1264 (1985).
17. J. Lahiri, S.T. Manson, Phys. Rev. A **48**, 3674 (1993).
18. D.E. Rothe, J. Quant. Spectrosc. Radiat. Transfer **11**, 355 (1971).
19. N.V. Karlov, B.B. Krynetskll, O.M. Stel'makh, Kvant. Elektron. (Moscow) **5**, 744 (1978) [Sov. J. Quant. Electron. **8**, 1305 (1978)].
20. W. Kleen, R. Müller, *Laser* (Springer-Verlag, Berlin, Heidelberg, 1969).
21. For instance, in a recent work on the $J = 1 \rightarrow J = 2$ transition of helium [22], modifications with respect to the models of [14] have been derived.
22. F. Pereira Dos Santos, F. Perales, J. Léonard, A. Sinatra, Jumming Wang, F. Saverio Pavone, E. Rasel, C.S. Unnikrshnan, M. Leduc, Eur. Phys. J. D **14**, 15 (2001).